IEEE Access
Multidisciplinary ⋮ Rapid Review ⋮ Open Access Journal

Received 12 November 2023, accepted 24 November 2023, date of publication 27 November 2023,
date of current version 18 December 2023.

Digital Object Identifier 10.1109/ACCESS.2023.3337151

RESEARCH ARTICLE

Development of a New 24-bit High-Performance Chipless RFID Tag for Accurate Identification in IoT Systems

KAWTHER MEKKI[1], (Graduate Student Member, IEEE), OMRANE NECIBI[2], NOUREDDINE BOULEJFEN[3], (Senior Member, IEEE), SAMIA LARGUECH[4], NORAH MUHAMMAD ALWADAI[5], AND ALI GHARSALLAH[1], (Senior Member, IEEE)

[1]Microwave Electronic Research Laboratory, Faculty of Science, University of Tunis El Manar, El Manar 2092, Tunisia
[2]Department of Computer Science, College of Arts and Sciences at Tabarjal, Jouf University, Jouf 72388, Saudi Arabia
[3]Centre for Research on Microelectronics and Nanotechnology, Sousse 4054, Tunisia
[4]Department of Electrical Engineering, College of Engineering, Princess Nourah bint Abdulrahman University, Riyadh 11671, Saudi Arabia
[5]Department of Physics, College of Sciences, Princess Nourah bint Abdulrahman University, Riyadh 11671, Saudi Arabia

Corresponding author: Kawther Mekki (kawther.mekki@gmail.com)

This work was supported by the Deanship of Scientific Research, Princess Nourah bint Abdulrahman University, Riyadh, Saudi Arabia, through the Program of Research Project Funding After Publication under Grant 44-PRFA-P-40.

ABSTRACT Chipless RFID has the potential to bring in a paradigm change in industrial applications, notably in the world of the Internet of Things (IoT). This wireless technology permits distant identification, sensing, and tracking, giving tremendous development prospects. Despite substantial advances over the previous century, designing high-performance chipless RFID for IoT applications remains a problem. This research presents a new chipless planar RFID tag for item tracking and identification in IoT systems. The suggested tag uses numerous T-shaped slow-wave structures as micro-reflecting resonators with different dimensions on a lossy substrate to encode information in the tag's backscattered signal after illumination. The mutual coupling between the resonators has been minimized to improve tag performance and printing variety. A tag with a coding capacity of 24 bits and a compact size of 60 × 40 mm^2 was simulated in CST Microwave Studio to validate the suggested approach. To create tags, several patterned configurations were applied on a Rogers RO4350B substrate, and their radar cross-section responses were studied. When compared to typical multi-resonator tags, the suggested tag design demonstrated excellent downsizing and efficient frequency spectrum usage. Furthermore, the Q-factor and coding strength were both high, showing that the suggested technology is capable of manufacturing high-performance chipless tags.

INDEX TERMS Internet of Things (IoT), chipless RFID tag, slow wave structure, RCS, resonators.

I. INTRODUCTION

The internet has now become an indispensable part of our daily life. It may be used for many things, including sharing, regulating, working, shopping, earning, and even learning. Furthermore, the internet's reach has extended beyond human interactions, linking innumerable items throughout the globe, culminating in a massive network with billions of nodes. This evolution gave birth to the IoT, which has emerged as a dynamic and developing phenomenon [1], [2], [3].

The associate editor coordinating the review of this manuscript and approving it for publication was Renato Ferrero.

The Internet of Things is made up of a slew of capable and intelligent things that surround us and communicate with one another depending on system requirements. These include environmental sensors, metering technology, and wearable technologies [4]. The rise of IoT systems is transforming regular, conventional objects into smart, networked entities, causing a profound upheaval in the global technology environment [5].

There is an urgent need for devices that have exceptional miniaturization, use minimal power, and are economical in order to increase the general adoption of an IoT system. Given this context, radiofrequency identification (RFID) emerges as

an attractive and generally accepted method for implementing Internet of Things systems or networks comprised of dispersed sensors. RFIDs are very inexpensive, have different identities, and have a broad range of sensing capabilities [6], [7]. Significant efforts have been made in recent years to reduce the cost of RFID tags. Nonetheless, it is certain that they will continue to be more expensive than barcode labels. The latter comprises simply printed paper, which is still required, while RFID incurs additional costs for the chip and antenna. The key to achieving a considerable cost decrease, reducing it below the predicted acceptability threshold of one cent, is to design RFID tags without an integrated chip. Chipless RFID is a fascinating approach that combines some RFID functions with the cost and simplicity of barcodes.

Chipless RFID includes a wide range of tags that may be classified into three main forms of coding: Chipless tags that operate in the time domain [8], [9], [10], [11], [12], [13], [14], chipless tags that operate in the frequency domain [15], [16], [17], [18], [19], and chipless tags that use hybrid coding [20], [21], [22], [23], [24].

The first chipless tags were inspired by typical RFID technology, in which coding is done in the time domain. Scholars have attempted to reproduce the temporal variations of the signal seen in the response frame of a conventional RFID tag. The fundamental problem in building a timing chipless tag is to build sufficiently long lines to cause observable delays while keeping the tag size small. There is also the problem of transmission line losses, which reduce the amplitude of reflections. Zheng et al. provided an instructive example of such a tag in 2004 [8]. This tag's coding capability is restricted to 4 bits inside an 8.2×3.1 cm^2 area. It uses the UWB frequency band, and its interrogation signal is a 2 ns pulse. The authors show how to customize the tags by adding material to particular areas using a conductive inkjet printer. This design, however, is inappropriate for consumer product traceability owing to its size. As a result of the inherent restrictions in encoding a considerable number of bits using a time tag, other applications such as localization [9] or the development of cheap passive sensors [10], [11] have been investigated. The authors of [12], [13], and [14] used a piezoelectric substrate to create SAW (Surface Acoustic Wave) based tags. These tags are major advancements in the industry since they are the first chipless tags published in the literature [12], showing the time domain coding concept. SAW tags use substantially less power at an equal reading distance than standard RFID tags, which depend on an adequate power source for activation and operation. This unique characteristic allows these tags to read from a few meters away. However, it is essential to highlight that the cost of SAW tags remains very high, prohibiting them from being used on low-priced materials such as paper.

The use of the tag's frequency signature serves as the basis for the second method used to encode information. This signature describes how the amplitude or phase of the tag response changes as the frequency changes. The encoding method is based on finding significant aspects within the spectral signature, such as peaks and troughs. In terms of coding capacity and density, scholars agree that frequency coding outperforms the temporal method. The concept of frequency tags was initially described in 2008 [15], and the first version used planar filters. The tag is made up of two broadband antennas coupled by a microstrip line. The tag produces dips in its spectrum response by putting spiral resonators of varied lengths along the line. These frequency dips, or the lack thereof, are used to encode and transmit data. The tag initially had a restricted coding capability of 6 bits. However, the same structure was improved in 2009 [16], resulting in a capacity of 35 bits for an area of 88×65 mm^2. This tag operates in the 3 to 7 GHz frequency spectrum, known as the UWB band, and has a meander-shaped transmission line with resonators on both sides. When compared to the previous version, this design change greatly minimizes the surface area occupied by the tag. [17] proposes a design that provides a coding capacity of around 5 bits using 5 resonators in a small area of approximately 25×30 mm^2. The required bandwidth ranges from 5.45 GHz to 5.85 GHz, corresponding to one bit per 100 MHz. Experiment results indicate that this tag, with a transmission power of 500 mW, may be detected from many tens of centimeters away. In 2012, [18] presented an alternate tag design based on the same principle. The FR4 substrate was used in its development, allowing it to operate without a ground plane at frequencies ranging from 2 to 4 GHz. The proposed tag consists of 20 resonators, each shaped like a C and serving as a basic coding particle. The tag, which has a capacity of 20 bits, can hold 1.14 bits per cm2 of data on a surface of 25×70 mm^2. Another tag, which exploits the concept of an elementary coding particle, was developed in separate research [19] in 2012. This tag has a ground plane, works in the UWB band, and is built on the Roger RO4003 substrate.

Hybrid coding was first described in the literature in 2012 [20], with the goal of increasing bit densities in the Chipless RFID tag domain while reducing tag area growth. This led to the creation of hybrid tags, which combine the frequency domain method with existing Chipless RFID tag designs [21], [22], [23]. In 2013, [24] offered an example of hybrid coding that used both the frequency and amplitude of a peak. The primary goal of this study was to develop a tag with a configuration that is undetectable to the human eye, solving anti-counterfeiting problems. The overall tag was made up of three resonators with a total surface area of 70×40 mm^2. Each resonator could encode four distinct amplitude states, for a total encoding capacity of six bits for the three resonators.

Despite the multiple benefits chipless RFID provides over standard RFID and other technologies, there is a dearth of evidence in the literature about chipless technology's broad use in the IoT era. The purpose of this study is to bridge the gap between chipless technology and IoT by focusing on the creation and implementation of low-cost chipless tags for IoT and other applications. IoT applications require efficient encoding and decoding of information. In this design, the

tag uses T-shaped slow-wave structures as micro-reflecting resonators on a lossy substrate to encode information in the tag's backscattered signal. This encoding method must be reliable and resistant to interference, crucial for IoT applications where data accuracy is vital. The tag is 60×40 mm^2 in size and has a coding capacity of 24 bits, which allows for a vast number of unique identifiers. This is important for item tracking and identification in IoT systems with a large number of assets. Error-free bit encoding for diverse bit patterns is done by providing a steady frequency response of the resonator design under varied situations, including in the presence or absence of adjacent elements. RFID tags operating within the indicated frequency range were produced and experimentally tested in an anechoic chamber utilizing a vector network analyzer (VNA) as an RFID transceiver to verify the proposed encoding/identification process. The results show that the 24-bit tags have deep nulls over the spectrum between 4 and 6.5 GHz, with an encoding density (D) of 9.6 bits/GHz, the highest ever obtained in chipless RFID. Furthermore, the measurements show a high-quality factor (Q-factor) and reliable coding, indicating that the method used in creating high-performance chipless tags was successful.

This paper is structured as follows: In Section II, we present an introduction to chipless RFID technology. Section III outlines the design methodology for the resonant elements employed in chipless tags. In Section IV, we lay out the whole design for the chipless tag. The experimental measurement data that was used to evaluate the proposed chipless tag's performance is presented in Section V. In Section VI, we evaluate the suggested tag in relation to similar tags that have been addressed in the literature. The results of this research are summarized in Section VII.

II. RADIO FREQUENCY IDENTIFICATION (RFID) SYSTEM OPERATING PRINCIPLES FOR CHIPLESS SYSTEM

The chipless RFID tag is the main component of the chipless RFID system, which also includes a reader antenna [25], [26], [27]. In contrast to conventional RFID systems, the chipless RFID system uses spectral signatures for data encoding, and the tags don't need a power source to function [28], [29], [30]. Figure 1 depicts a simplified representation of the chipless RFID system configuration.

The multi-resonators tag's interrogation signal is picked up by the reader antenna. The spectrum of the interrogation signal provided by the reader is modulated using a multi-resonator, which is made up of a number of filtering sections. On the spectrum's amplitude and phase, the modulation is applied. At the resonant frequency of the multi-resonators, the amplitude and phase are modulated as amplitude attenuations and phase leaps, respectively. When a chipless RFID tag enters the reader's interrogation zone, the electronic chipless RFID reader may determine the identification of the tag. The chipless tag's identity may be found via the RFID reader's detection and decoding of RFID tags [31], [32].

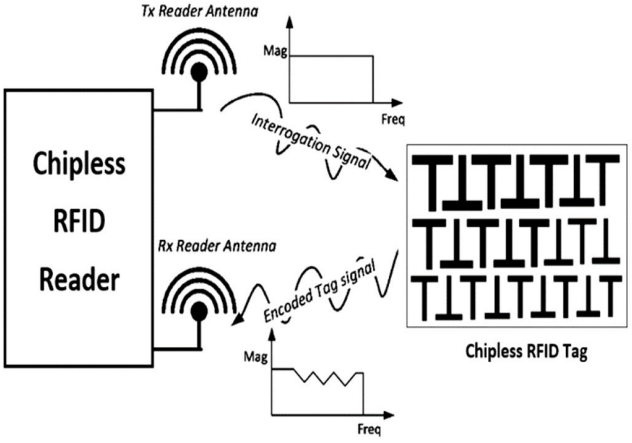

FIGURE 1. The operating principle of the RFID system chipless.

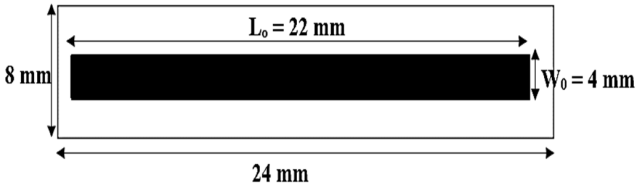

FIGURE 2. The basic design of a half-wave dipole resonator.

III. RESONANT ELEMENT DESIGN

A. BASIC STRUCTURE

This article describes an RCS-based tag that uses a linearly polarized planar wave to stimulate a total of 24 reflecting resonators. The tag code represents the spectral signature that the reflecting resonators produce. Because they receive the signal and return it with the tag signature, the reflecting resonators are crucial in identifying the planar chipless RFID tag. Figure 2 shows the tag's half-wave dipole reflecting resonator.

Considering that fres is the resonant frequency in the substrate, then the length of the reflecting dipole resonator is $\lambda g/2$, with λg being the wavelength. According to [33], fres is unaffected by linewidth. Reduced linewidth, on the other hand, results in a higher resonance Q-factor. Computer Simulation Technology (CST) Studio Suite was used to simulate a half-wave dipole reflecting resonator with dimensions of $L_0 = 22$ mm and $W_0 = 4$ mm, with a resonant frequency of fres $= 4.1$ GHz, and a Rogers RO4003C substrate with thickness h $= 0.41$ mm, dielectric constant $\varepsilon_r = 3.38$ and loss tangent tg$\delta = 0.0019$.

Figure 3 shows the radiation pattern and RCS response of a half-wave dipole reflecting resonator operating at 4.1GHz. The simulation results show an omnidirectional radiation pattern in the plane perpendicular to the dipole axis. This feature is important for RFID applications as it allows the detection of reflected waves regardless of the orientation of the resonator.

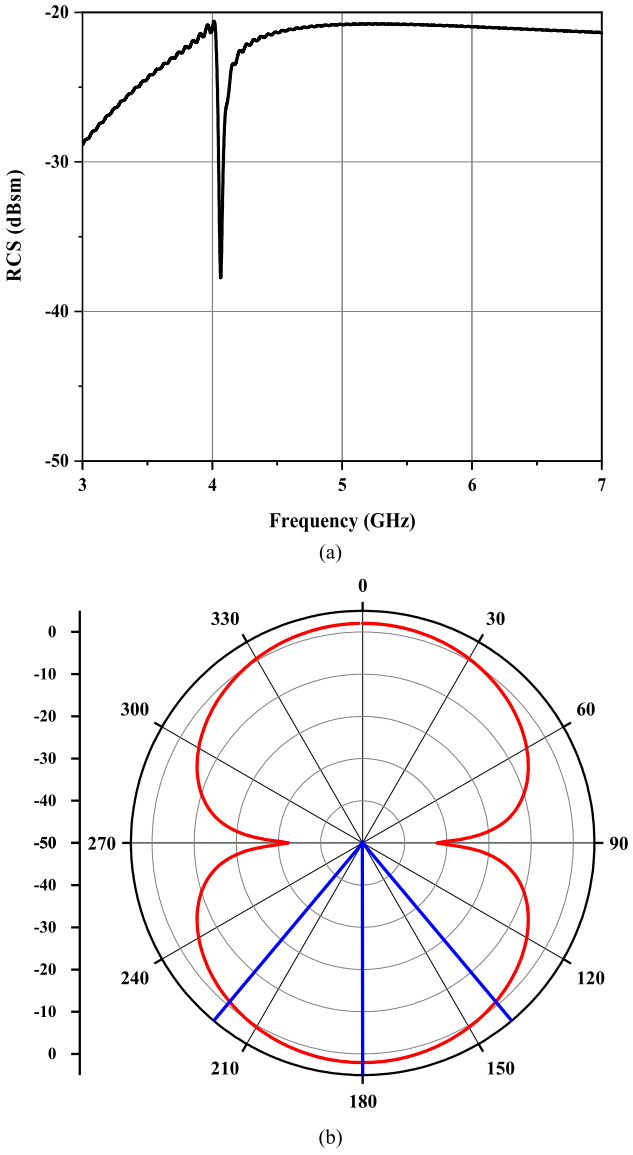

FIGURE 3. The simulation results of the basic half-wave dipole reflecting resonator, (a) the RCS response and (b) the radiation pattern.

These classical reflecting resonators, suffer from poor quality factors and big dimensions leading to large footprints. Many studies have focused on using structures to lower the wave's phase velocity in order to accomplish the dual goals of low losses and high downsizing [34], [35], [36], [37]. Using high permittivity substrates or by altering the propagation line's shape, the slow wave effect may be explained in terms of the confinement of the created electric and magnetic fields.

The electrical properties of a half-wave dipole define its behavior: the characteristic impedance Z_{c_un} and the propagation exponent γ such that:

$$Z_{c\_un} = \sqrt{\frac{R + jL\omega}{G + jC\omega}} \tag{1}$$

$$\gamma = \sqrt{((R + jL\omega)(G + jC\omega))} = \alpha + j\beta \tag{2}$$

where α is the attenuation exponent in Np. m^{-1}, R, L, G and C are the per-unit-length RLGC parameters and β is the phase exponent or Linear phase shift in rad. m^{-1} of a lossy microstrip line.

In general, equation 1 provides a complex representation of a microstrip line's characteristic impedance. However, in practice, the quality of the used conductor (Copper, Gold or Silver) as well as the dielectric substrates most often place us, in the RF domain, in a "low loss" context which implies that: $R \ll jL\omega$ and $G \ll jC\omega$. We then consider the lossless case such that:

$$Z_{c\_un} = \sqrt{\frac{L}{C}} \tag{3}$$

Transmission line characteristics such as wave phase velocity V_{p_un} and guided wavelength λ are also critical.

$$V_{p\_un} = \frac{C_0}{\sqrt{\varepsilon_{reff}}\sqrt{\mu_{reff}}} = \lambda \times f = \frac{1}{\sqrt{L \times C}} \tag{4}$$

where f is the operating frequency, C_0 is the speed of light in vacuum and ε_{reff} and μ_{reff} represent the effective relative permittivity and permeability respectively. The physical length of a reflecting resonator is critical since it affects the overall chip area. To reduce the length of the half-wave dipole reflecting resonator but maintain its electrical characteristics, a slow-wave structure was devised, which is based on the fundamental structure previously outlined.

B. MINIATURIZATION OF THE HALF-WAVE DIPOLE REFLECTING RESONATOR BY ADDING A CAPACITIVE ELEMENT

A standard microstrip line of a specific length is replaced by a microstrip line loaded with a capacitive element, as shown in Figure 4, based on the slow-wave principle.

The reduction of the physical length of the reflecting resonators allows reduced losses, leading to low noise in the RF receiving chain. The design challenge is not only to reduce the length, which requires modification of the original structure, but also to maintain or even increase the quality factor.

In order to miniaturize the reflecting resonators, one can either artificially increase the linear inductance (L) and/or the linear capacitance (C) of the line, or utilize substrates with high relative permittivity (ε_{reff}).

The process of "line miniaturization" entails changing a line's geometry and rate of wave propagation. It is based on a simple scientific observation: storing electrical or magnetic energy increases the linear capacity (C) and/or the linear inductance (L) of the line, delaying wave propagation relative to the classical directed propagation of the electromagnetic field.

Placing a capacitive load on a stub is an innovative technique for reducing line size. Figure 4 shows the use of a stub to load a half-wave dipole in an open circuit. The existence of the stub introduces an equivalent capacitance, Cp, which is dictated by the stub's size.

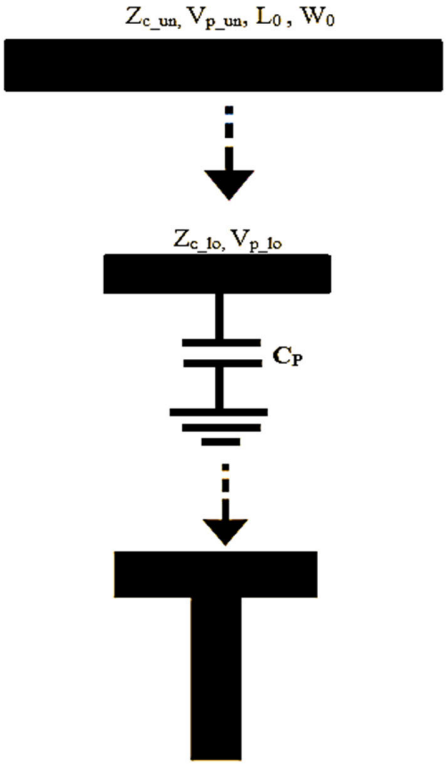

FIGURE 4. The premise of the slow-wave approach.

The transmission line's characteristic impedance and phase velocity may be reduced by loading it with a shunt capacitor. The loaded characteristic impedance Z_{c_lo} and phase velocity V_{p_lo} of the stub are provided in [37] as:

$$Z_{c\_l0} = \sqrt{\frac{L}{C+C_p}} \tag{5}$$

$$V_{p\_l0} = \frac{1}{\sqrt{L(C+C_p)}} \tag{6}$$

Equation (6) illustrates how the phase velocity V_{p_lo} is lowered in comparison to an unloaded line. This means that a transmission line with a shortened physical length can achieve an electrical length equivalent to that of a line with its original, unmodified length. In a line whose dielectric is air or vacuum (permittivity ($\varepsilon_{reff} = 1$)) the electric current moves practically at the speed of light ($C_0 = 300000$ km/s). For any other dielectric, the signal propagation speed (v) is less than (C_0) such that:

$$v = \frac{1}{\sqrt{\varepsilon_{reff}}} C_0 = V_f \times C_0 \tag{7}$$

$$V_f = \frac{1}{\sqrt{\varepsilon_{reff}}} \tag{8}$$

Equation (9) gives the electrical length of a line knowing its physical length and its velocity coefficient.

$$\emptyset_{lo} = \frac{L_{phy}}{V_f} \tag{9}$$

where $L_{phy} L_{phy}$ is the physical length of the line and V_f is the velocity coefficient, which is always less than 1.

The effective electrical length of the loaded line is computed using the following method:

$$\emptyset_{lo} = \frac{N\omega_0}{V_{p\_l0}} = N\omega_0\sqrt{L(C+C_p)} \tag{10}$$

N stands for the number of loading capacitors, while ω_0 stands for the preferred angular frequency. Equations (3) through (10) may be used to calculate the capacitance Cp of the loading capacitor, ensuring that:

$$C_p = \frac{\emptyset_{l0}(Z_{c\_un}2 - Z_{c\_l0}2)}{N\omega_0 Z_{c\_un}2Z_{c\_l0}} \tag{11}$$

The equivalent capacitance is defined by the stub length as well as the characteristic impedance. The characteristic impedance of the loaded propagation line section must be bigger than the characteristic impedance of the equivalent unloaded line ($Z_{c\_lo} > Z_{c\_un}$) to get an insignificant equivalent propagation line while keeping the same propagation characteristics at a given frequency.

As a consequence, to achieve the largest possible length reduction, it is preferable to have a big gap between the loaded (Z_{c_lo}) and unloaded (Z_{c_un}) characteristic impedances. Furthermore, by decreasing the stub's characteristic impedance and therefore increasing its width up to a particular threshold, the stub's length may be reduced further and the coupling between the elements eliminated. By taking into account all these design considerations, it is possible to construct a slow-wave structure-based reflecting resonator that is smaller than the fundamental half-wave dipole reflecting resonator, while preserving the same electrical and radiating properties. To obtain the greatest possible decrease in line length, the characteristic impedance (Z_{c_un}) of the fundamental half-wave dipole resonator must be minimized. This explains why the width $W_0 = 4$ mm (Figure 2), which has a characteristic impedance $Z_{c\_un} = 27.8$ ohm and a resonance Q-factor that is acceptable, was chosen. Aside from that, the loaded microstrip line impedance Z_{c_lo} should be set to the maximum possible value. Consequently, the linewidth of the loaded microstrip line is set at $G_1 = 3$ mm, resulting in a characteristic impedance of roughly $Z_{c\_lo} = 34$ ohm for the device. The characteristics of a reflecting resonator based on a slow wave were derived using Equations (1)-(11), with the same behavior and frequency response as the fundamental half-wave dipole. So, the unloaded micro-strip line must be loaded with $N = 1$ capacitances of $Cp = 1.1$ pF.

The simulation was carried out primarily to test the efficiency of the slow-wave approach used in the design of the reflecting resonator. The simulation results in Figure 5 demonstrate that the RCS responses and radiation patterns of the basic half-wave dipole reflecting resonator and its slow-wave-based equivalent are identical. An approximate resonant frequency of around 4.1 GHz was observed in the RCS response of the developed slow-wave-based reflecting resonator, which is consistent with the resonant frequency of

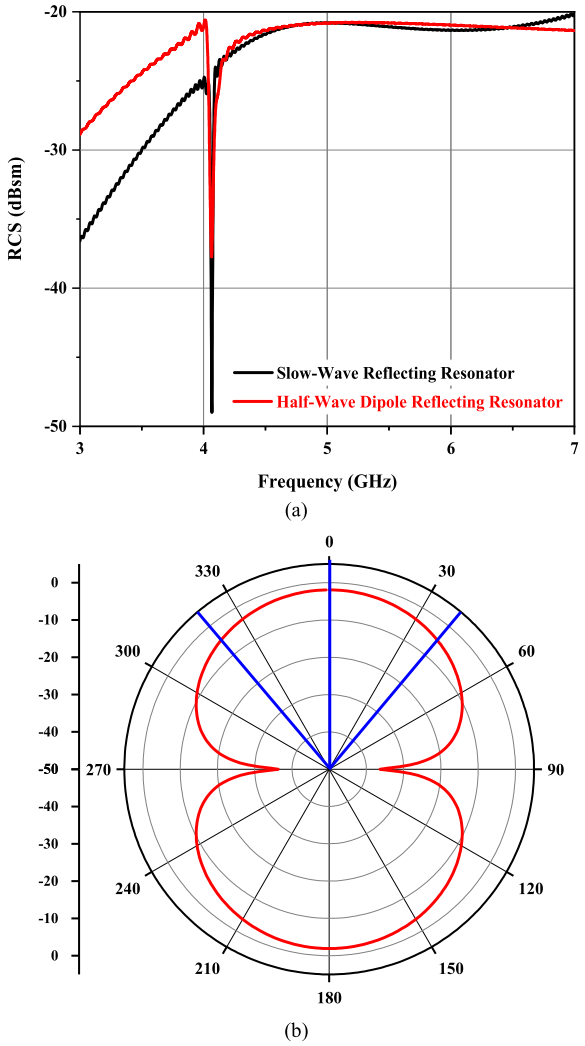

FIGURE 5. The simulation results: (a) the RCS responses of the slow-wave-based and half-wave dipole reflecting resonators, (b) the radiation pattern of the slow-wave reflecting resonator.

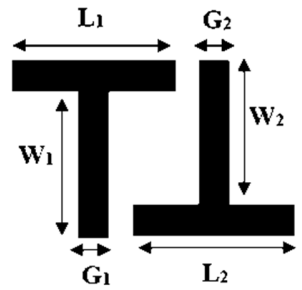

FIGURE 6. Tag designed with two different bit resonators for state '11'.

TABLE 1. Parameters of the different resonances in Figure 6.

Parameter	L_1	W_1	G_1	L_2	W_2	G_2
Value (mm)	12	12.4	3	11.75	12.2	3

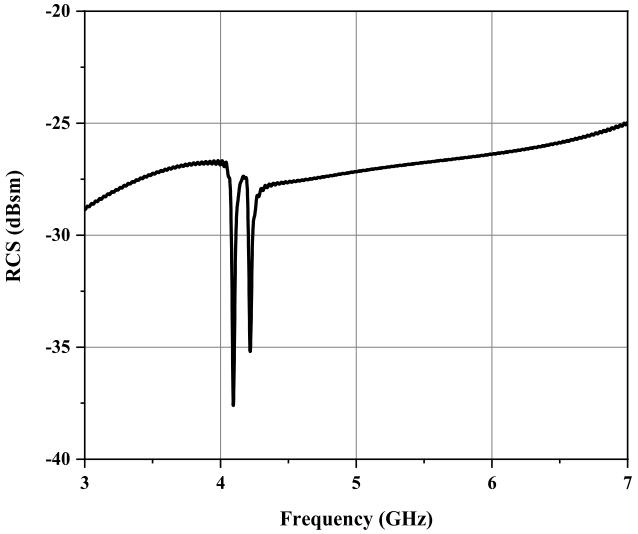

FIGURE 7. Simulated RCS magnitude for the "11" states.

the basic half-wave dipole reflecting resonator. As a result, there is a strong correlation in the RCS responses of the two investigated resonators. As shown in Figure 5(b), it is easily comparable to the performance of the half-wave dipole reflecting resonator depicted in Figure 3(b). It was noted in the radiation pattern, that the omnidirectional radiation was preserved.

The figure reveals that the slow-wave structure exhibited a higher Q-factor in comparison to that of the half wave dipole. This improves tag pattern bit value detection and recognition. The results obtained demonstrate the effectiveness of the slow-wave structure, which resulted in improved electrical and radiating performances while reducing the length of the resonator by 40%.

IV. OVERALL CHIPLESS RFID TAG DESIGN

A. DESIGN AND ELECTROMAGNETIC SIMULATIONS

An RCS-based chipless tag was developed using 24 slow-wave reflecting resonators operating in the C frequency range, since the effectiveness of using a slow-wave approach to minimize the length of a single reflecting resonator was established through validation. It is anticipated that the proposed tag would be less in total length, while an increase in the tag width is anticipated due to the shunted stub.

Initially, a new T-shaped resonator is created to achieve a resonance frequency in the desired frequency range. Then, another T-shaped resonator is placed head-to-tail as shown in Figure 6, with the intention of enhancing the overall tag dimensions.

Table 1 shows the dimensions of the first and second resonators.

Figure 7 depicts the magnitude response of the tag's RCS.There are two resonance frequencies presented, f1 = 4.1 GHz and f2 = 4.2 GHz.

Figure 8, shows a 24-bit tag based on a slow-wave structure. The used resonators are placed in three lines with seven,

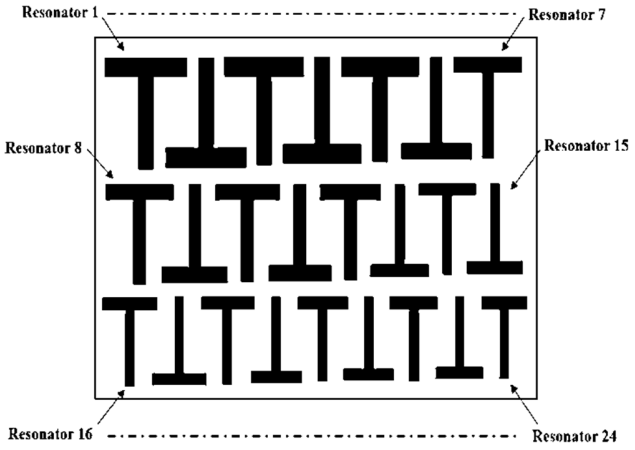

FIGURE 8. A chipless RFID tag with a 24-bit capacity that employs a slow wave structure.

eight, and nine resonators. The twenty-four resonators, each of which varies in length and width, exhibit twenty-four resonant frequencies that correlate to one another in order from longest to shortest. T-shaped and inverted T-shaped resonators may be added to or removed from the system throughout. This procedure is used to raise or reduce the total number of resonators present.

Table 2 shows the resonator dimensions for each bit position. These dimensions were parametrically designed to keep the tag's operating frequency band between 4 and 6.5 GHz, guaranteeing a high spectral and bit density.

The T-shaped chipless tag was developed with the goal of simplifying its design and production in order to maximize its use. Its overall size was 60 millimeters by 40 millimeters, the resonators that would be used for the 24-bit encoding were designed. Figure 9 depicts the arrangement used to simulate the chipless RFID tag. A plane wave with either vertical or horizontal polarization has the potential to activate the tag. The backscatter field is received in each scenario, and the frequency signature of the tag may be determined using the RCS magnitude. When the tag is activated by waves that are both vertically and horizontally polarized, RCS may then be determined.

In the majority of cases, these waves will make contact with the chipless RFID tag's surface. When the plane wave excites the tag, a considerably higher surface current is created around the resonators at their most significant resonant frequency. Using these orthogonal polarities has the potential to increase coding capacity. CST was employed in the design and simulation of the proposed tag.

The simulated RCS replies of the tags created for the various given tag codes are shown in Figure 10. Each of the reflecting resonators has a unique resonant frequency corresponding to 1 bit of the tag's code which is 111111111111111111111. The tag has a 24-resonance spectral signature, allowing it to encode information with a 24-bit capacity. The resonance frequencies fall between 4 and 6.5 GHz, with a frequency separation of around 100 MHz.

TABLE 2. Resonant frequencies and dimensions of the 24 resonators.

Resonator (from top to bottom)	Resonance Frequency (GHz)	L_i (mm)	W_i (mm)	G_i (mm)
Resonator 1	4.1	12	12.4	3
Resonator 2	4.2	11.75	12.2	3
Resonator 3	4.3	11.5	12	3
Resonator 4	4.4	11.25	11.8	3
Resonator 5	4.5	11	11.6	3
Resonator 6	4.6	10.75	11.4	3
Resonator 7	4.7	10.5	11.2	3
Resonator 8	4.8	10.25	11	3
Resonator 9	4.9	10	10.8	2.5
Resonator 10	5	9.75	10.6	2.5
Resonator 11	5.1	9.5	10.4	2.5
Resonator 12	5.2	925	10.2	2.5
Resonator 13	5.3	9	10	2.5
Resonator 14	5.4	8.75	9.8	2.5
Resonator 15	5.5	8.5	9.6	2.5
Resonator 16	5.6	8.25	9.4	2.5
Resonator 17	5.7	8	9.2	2
Resonator 18	5.8	7.75	9	2
Resonator 19	5.9	7.5	8.8	2
Resonator 20	6	7.25	8.6	2
Resonator 21	6.1	7	8.4	2
Resonator 22	6.2	6.75	8.2	2
Resonator 23	6.3	6.5	8	2
Resonator 24	6.4	6.25	7.8	2

Figure 11 depicts the recorded backscattered signal responses from the tag when a linearly polarized wave emitted by the reader interacts with the tag. It clearly reveals the existence of twenty-four distinct resonance signatures, that in turn points to a one-of-a-kind 24-bit identification. The frequency signatures exhibit the resonators' exceptional quality factor, which enables precise data reading from the tag.

B. STRUCTURE OF CHIPLESS TAGS USING DIFFERENT CODES

The electromagnetic characteristics of the previously mentioned tags with distinct codes were simulated, and Figure 12

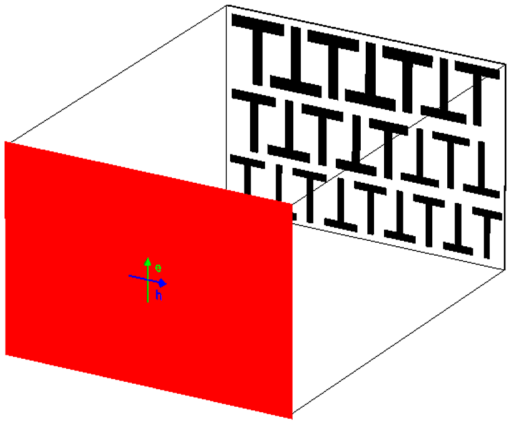

FIGURE 9. Simulation configuration for the suggested tag.

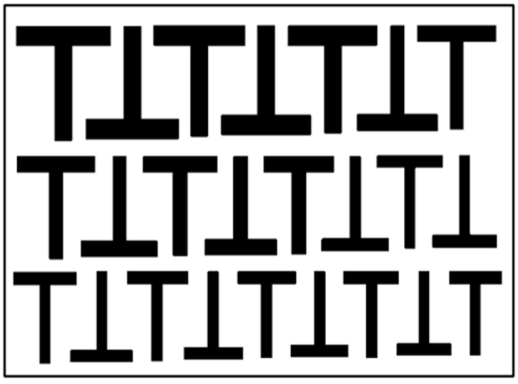

FIGURE 10. Tag designed with two different bit combinations "1111111111111111111111111".

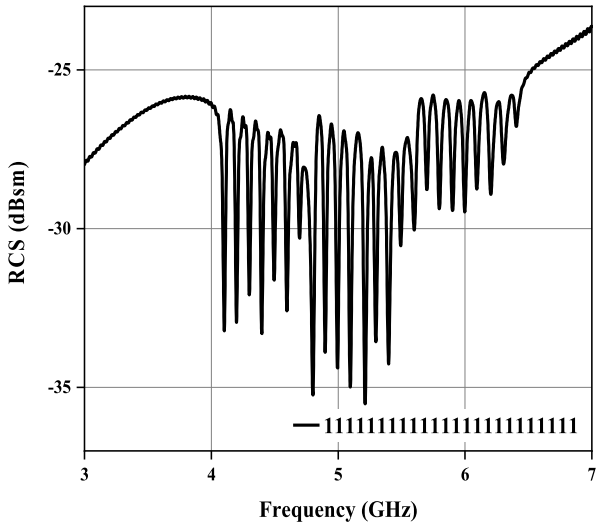

FIGURE 11. Simulated RCS magnitude for the states "1111111111111111111111111".

illustrates the tag that has been created using two distinct bit combinations. In the proposed tag's on-off keying coding technique, the presence of a resonant frequency corresponds to a bit being set to 1, indicating its existence.

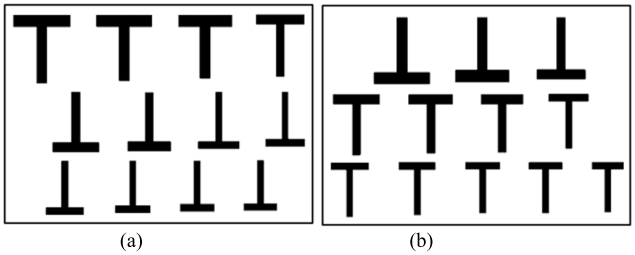

FIGURE 12. Tag designed with two distinct bit combinations: (a) "10101010101010101010101010" and (b) "01010101010101010101010101".

On the other hand, the absence of a resonant frequency represents a bit being set to 0, indicating its non-existence. To adjust the tag code by setting specific bits to zero, the reflecting resonators that correspond to those bits must be deleted. Figure 12(a) illustrates the layouts of the tags with the numbers 10101010101010101010, and Figure 12(b) depicts the same information for the tags with the codes 01010101010101010101010101.

The Figure 13(a) and 13(b) clearly demonstrate this, for the black curve, all resonance frequencies are present, which is in accordance with the tag code set to "1111111111111111111111111," while there are missing resonance frequencies for the pink and red curves according to the corresponding tag codes "10101010101010101010 10" and "01010101010101010101010101" as the frequency responses are with alternating ones and zeros. These two curves make it very evident that the resonance frequencies related the bits set to 0 have been eliminated, whereas the resonance frequencies associated with the bits set to 1 remain unchanged.

Figure 13 demonstrates that each of the resonances has a strong Q-factor, and regardless of whether or not the tag code is altered, each of the fixed resonances maintains its original frequency position. The proposed tag clearly demonstrates an effective coding strategy and a high level of identification.

C. DESIGN CHIPLESS TAG WITH REARRANGED RESONATORS

Because of the closer proximity of the resonators, there is a possibility of mutual coupling, which causes the responses of the surrounding resonators in the tag to become detuned. The researchers utilized an approach that is outlined in [38] and [39] and is meant to limit the amount of inter-resonator mutual coupling. The goal of this strategy is to ensure that the locations of the peaks do not vary regardless of the tag that is being used.

The reflecting resonators were altered in order to maintain a sufficient distance between each pair of reflecting resonators with close resonance frequencies. In order to separate two reflecting resonators with close resonance frequencies, they were reorganized horizontally and vertically, as shown in Figure 14 and Figure 16. This was done in order to get the desired result.

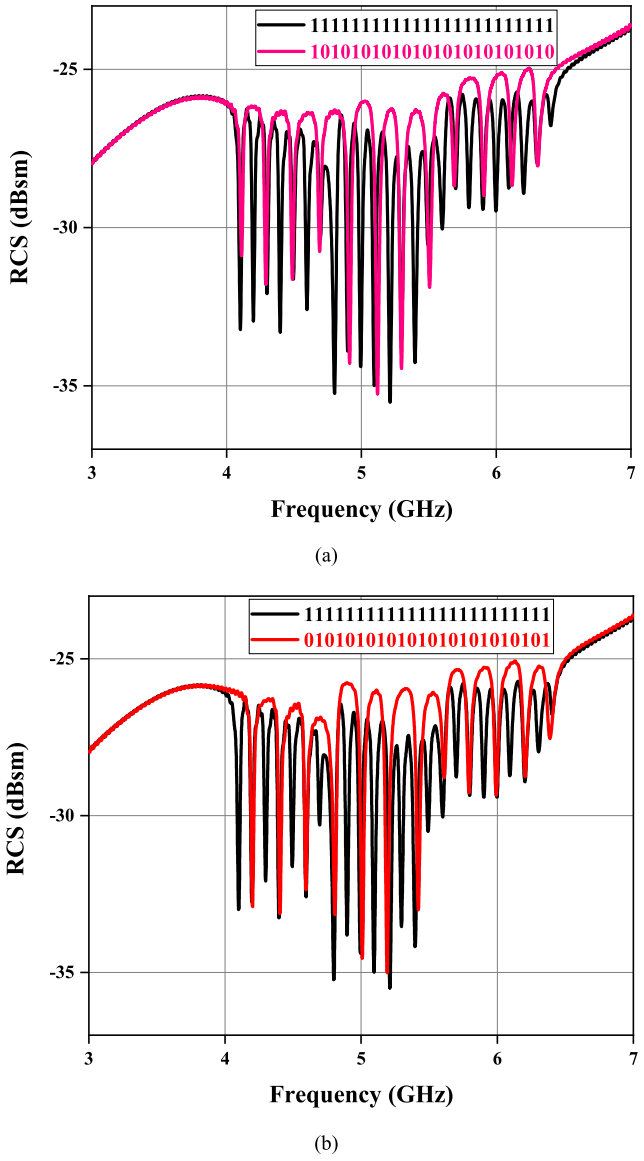

FIGURE 13. Simulated RCS magnitude for the states: (a) "101010101010101010101010" and (b) "010101010101010101010101".

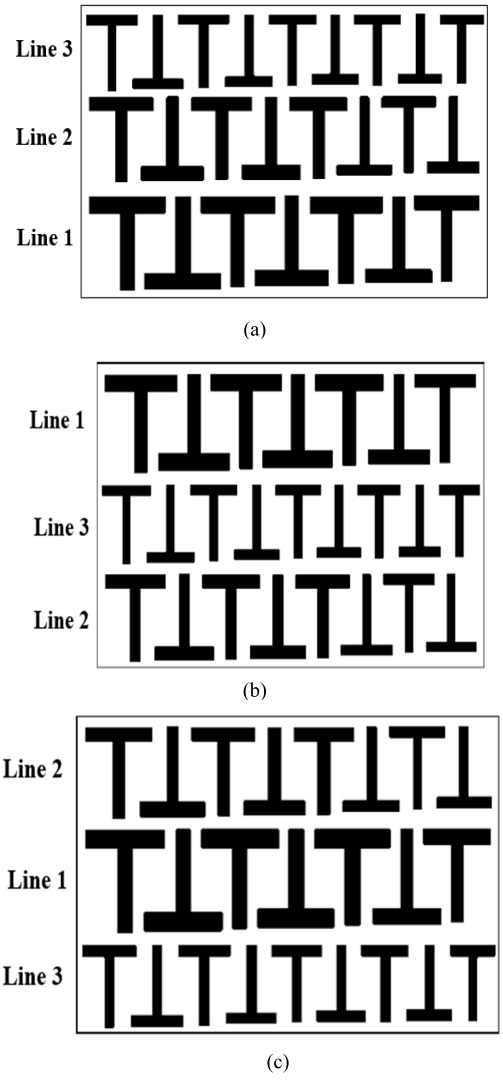

FIGURE 14. The horizontally rearranged resonators: (a) line 3 and line 1, (b) line 3 and line 2, (c) line 2 and line 1.

Horizontally, the original ascending sequence of resonator lines Line 1, Line 2, and Line 3 has been changed to Line 3, Line 2, and Line 1, followed by Line 1, Line 3 and Line 2, and finally Line 2, Line 1 and Line 3.

The RCS simulation result in Figure 15 was implemented from the new designed tags with the resonators rearranged horizontally (line 3 and line 1, line 3 and line 2, line 2 and line 1) has been performed for the three tags. In this configuration, the level of the RCS changes depending on the shape of each resonator without changing the positions of the RCS peaks.

Vertically, the original ascending order of resonators res 1 to res 7, res 8 to res 15 and res 16 to res 24 is adjusted to res 3, res 2, res 1, res 6, res 5, res 7, res 8, res 9, res 12, res 11, res 10, res 15, res 14, res 13, res 16, res 19, res 18, res 17, res 20, res 21, res 24, res 23, and res 22 [see Figure 16(a)].

The comparison of the RCS responses of the tags using the original resonator configuration and those with the new configuration is presented in Figure 16(b). The resulting structure maintained the same frequencies of resonance compared to those of the original one.

D. IMPACT OF TAG ORIENTATION

This is an extremely important feature for any RFID tag as it can be useful for important applications such as tagging of items in a supermarket or a sensor in the IoT framework. Such applications can be aided to a great extent by orientation tags. It is due to the fact that these applications may have tags in any orientation and still need to be read accurately. To discuss the orientation independence of the tag, a simulation framework was developed to assess the RCS magnitude at various orientations of the tags in CST software. The tag was positioned in opposition to the x, y, and z directions,

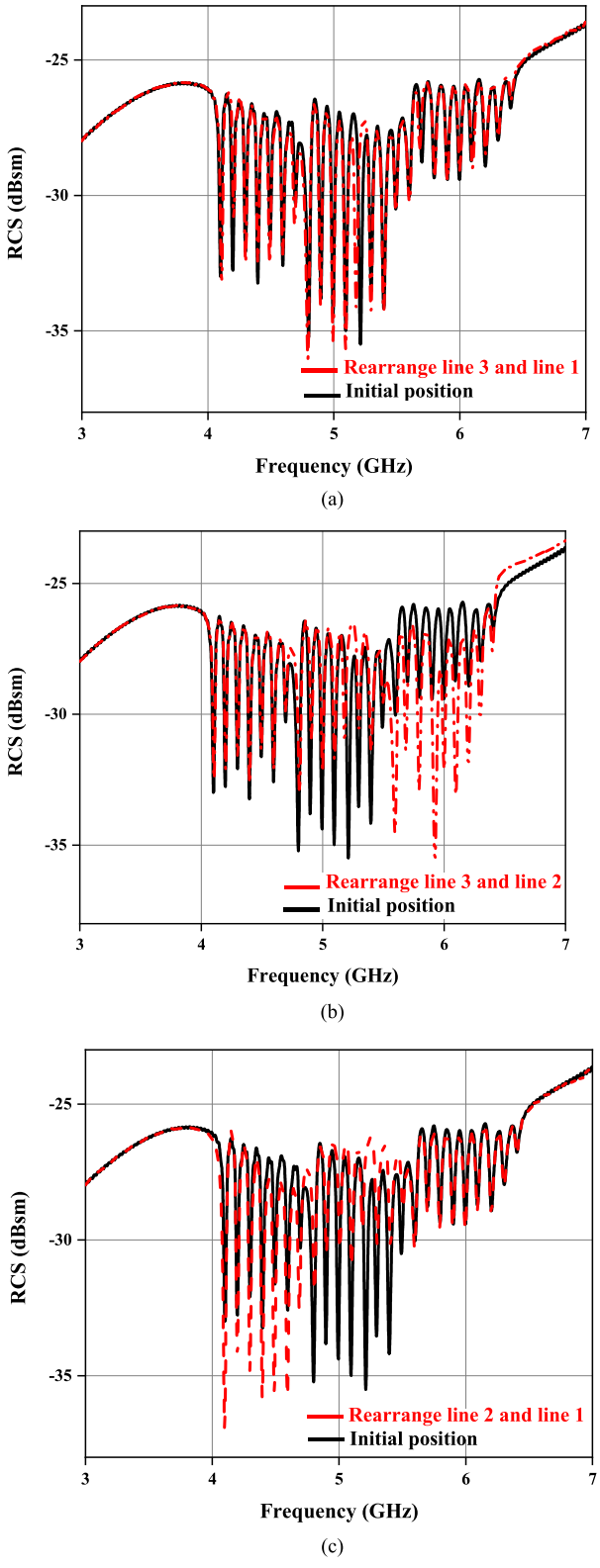

FIGURE 15. Simulated responses of the designed tag's RCS with rearranged resonators: (a) line 3 and line 1, (b) line 3 and line 2, (c) line 2 and line 1.

undergoing rotations of 20°, 40°, and 60° around the z-axis, as illustrated in Figure 17(a). The results for orientations at

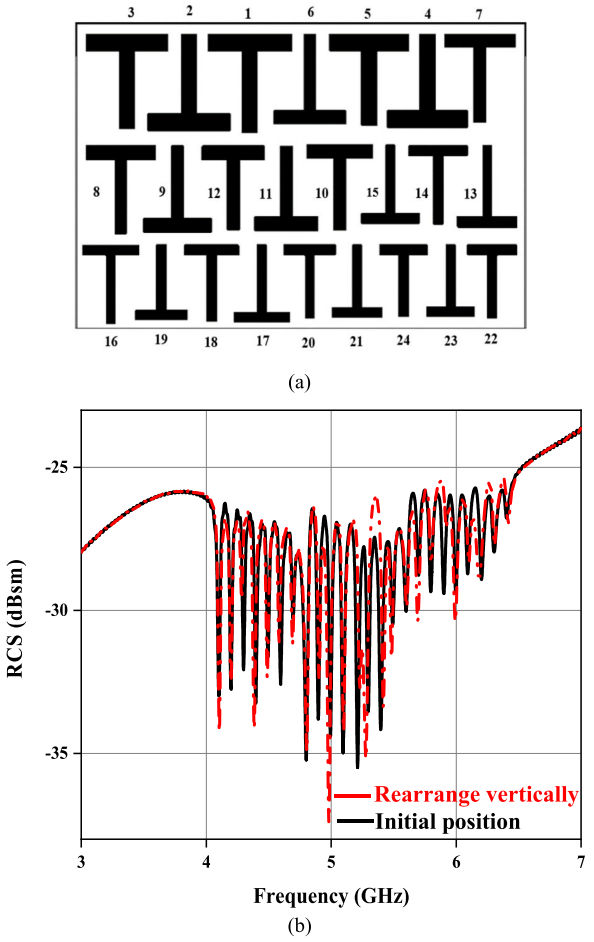

FIGURE 16. (a) The vertically rearranged resonators, (b) Simulated RCS responses.

20°, 40°, and 60° are illustrated in Figure 17(b), revealing a total of twenty-four resonant spectral peaks across different tag positions. The simulation outcomes reveal minor frequency shifts of approximately 10 MHz when the rotation angles (θ) are set at 20 and 30°. As the rotation angle surpasses 60°, there is a noticeable increase in frequency shifts, reaching around 30 MHz in the resonant frequencies across all orientations, particularly in the worst-case scenario. It is noteworthy, however, that these shifts do not compromise the reading capability of the tags. This is attributed to the preservation of sharpness and the narrowband characteristics of the signatures, ensuring their integrity despite the observed shifts.

Efficient utilization of the frequency spectrum is crucial in IoT applications to avoid interference and optimize network performance which enables a simple code identification and, therefore, a high level of coding robustness. The design aims to use the frequency spectrum efficiently, ensuring that the tag does not cause interference with other IoT devices operating in the same frequency range.

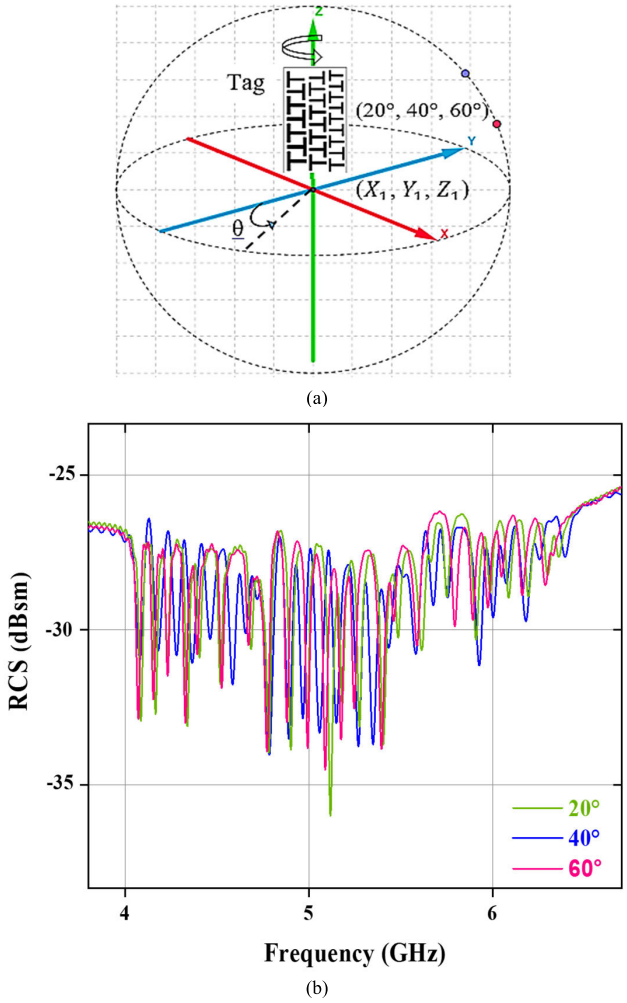

FIGURE 17. (a) Position of the tag with the rotation about the z-axis., (b) Magnitude response of RCS for various tag orientations.

V. EXPERIMENTAL VALIDATION

The proposed RCS-based chipless tag appears to work well based on simulation findings. The effectiveness of the suggested structure and the method used must, however, be confirmed and validated through experimental testing. The Rogers RO4350B substrate was used to realize the suggested prototype, which is then tested in an anechoic chamber (Figure 18).

Either a monostatic or a bistatic reading device may be used to read the information contained in chipless RFID tags. One antenna is used for the transmission while a second one is used for reception in bistatic systems, which employ two antennas. Monostatic systems, on the other hand, need only one antenna to perform both interrogation and readout functions; as a result, they are often more cost-effective than bistatic systems. By employing a monostatic setup, the influence of mutual coupling between the transmitting and receiving antennas is eliminated, and the need for employing an angle-dependent formula for the reference scatterer is avoided.

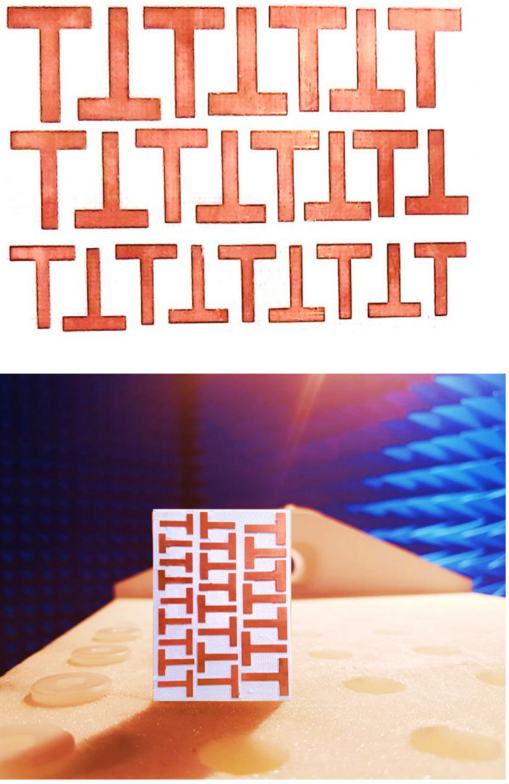

FIGURE 18. The proposed prototype of the chipless RFID tag.

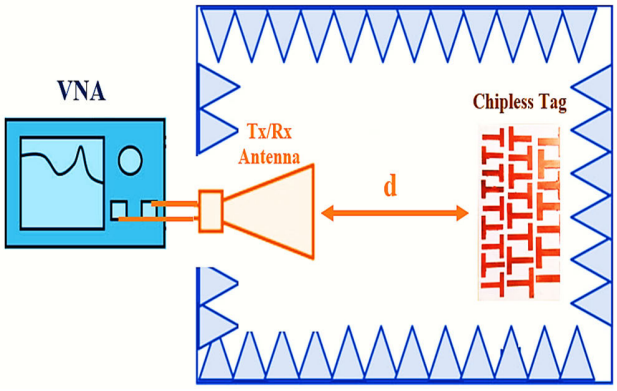

FIGURE 19. Measurement setup using a PNA5221A VNA.

The tag has been examined in an anechoic environment using a PNA5221A network analyzer and a monostatic measurement. As shown in Figure 19. The tag was based on the evaluation of the reflection coefficient of a double-ridged horn antenna QRH 20, the tags were placed at a distance of 15 cm in front of the horn antenna. The RCS response of the tag was calculated using relations given in [40] as:

$$\sigma^{tag} = 20\log\left[\frac{S_{11}^{tag} - S_{11}^{iso}}{S_{11}^{ref} - S_{11}^{iso}}\right]\sigma^{ref} \tag{12}$$

S_{11}^{tag} denotes the reflection coefficient observed when employing the measured tag as a scattering object.

TABLE 3. Comparing the proposed tag to existing tags in the literature.

Reference	Fequency Range (GHz)	Overall size of tag (L x W mm^2)	RCS level (dBsm)	Capacity (bits)	Spatial density (bit/cm^2)	Spectral capacity (bit/GHz)	Spatial density at center freq. (bit/λ^2)	Encoding capacity (bit/cm^2/GHz)	Encoding capacity (bit/λ^2/GHz)	Verification of 0-b Coding/ Resonance stability
[41]	3.5-6	20 x 20	-30	4	1	1.6	95.7	0.96	38.28	No
[42]	6-12	20 x 20	-35	8	2	1.3	41.1	0.6	6.85	Yes / No
[43]	4-9	25 x 25	-15	5	0.8	1	21.3	0.2	4.26	Yes / No
[44]	1.8-3.6	55 x 55	-33	20	0.66	11.11	81.5	0.37	45.27	Yes / Yes
[45]	6-12	21 x 21	-26	18	4.08	3	45.29	0.68	7.45	Yes / No
[46]	3-7	55 x 55	-55	8	0.26	2	7.2	0.05	1.8	No
[47]	2-5	40 x 40	-35	5	0.31	1.7	24.5	0.11	8.2	No
[48]	2-5	45 x 45	-16	4	0.2	1.33	14.49	0.07	4.83	No
[49]	4-6.5	60 x 40	-28	6	0.25	2.4	2.04	0.1	0.81	Yes / Yes
[50]	3-6	20 x 20	-40	8	2	2.66	88.67	0.66	29.55	Yes / Yes
[51]	8.3-12	15 x 21	-25	16	5	4.3	44.6	1.3	12	Yes / No
[52]	3-9	30 x 30	-20	23.7	2.6	3.95	49.67	0.43	8.33	No
[53]	7-11	30 x 30	-20	16	1.77	4	19.66	0.44	4.91	Yes / Yes
[54]	5.4-10.4	13.5 x 13.5	-35	10	5.44	2	78.44	1.088	15.68	Yes / No
[55]	2.5-8	30 x 30	-20	5	0.55	0.9	17.95	0.1	3.26	Yes / No
This work	4-6.5	60 x 40	-27	24	1	9.6	36	0.5	18	Yes / Yes

Conversely, S_{11}^{ref} signifies the reflection coefficient obtained with a reference metallic plate serving as the scatterer. Meanwhile, S_{11}^{iso} stands for the reflection coefficient originating solely from the antenna itself, devoid of any scatterer, accounting for residual reflections from the experimental environment.

Lastly, σ_{tag} represents the RCS of the measured tag, while σ_{ref} corresponds to the RCS of the reference scatterer. The reference scatterer in question is a rectangular metal plate with dimensions a $\times$ b $=$ 60 $\times$ 40 mm^2, akin to those of the measured tag, and possesses a thickness of 0.3 mm. The analytical expression for calculating the RCS of the reference scatterer can be found in [40].

$$\sigma^{ref} = 4\pi \frac{a^2 b^2}{\lambda^2} \tag{13}$$

λ represents the wavelength of the signal in a vacuum.

The response of the RCS for the tag, where the tag code is set to '1111111111111111111111' has been measured and compared to the simulated results. For better comparison, Figure 20 showcases both the simulated and measured RCS responses.

The two responses show a high level of consistency. Despite the slight shift in the resonance frequencies to higher frequencies, a total of 24 resonances were successfully detected within the frequency range of 4 GHz to 6.5 GHz, satisfying the specifications of the proposed tag. As a result, the re-arrangement technique successfully demonstrated its

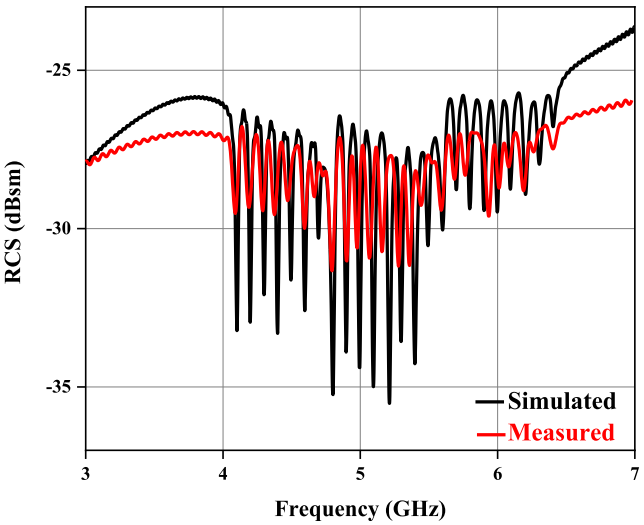

FIGURE 20. The measured RCS responses of the designed tags with 24-bits.

effectiveness by minimizing the mutual coupling between resonators.

VI. COMPARISON BETWEEN THE PROPOSED TAG AND DIFFERENT TAGS IN THE LITERATURE

To showcase the effectiveness of the slow-wave method, which is the miniaturization technique employed in this article, a comparative analysis was conducted between the newly proposed tag and an existing tag. The comparison encompasses numerous widely cited instances of chipless RFID tags in the frequency domain, and the results are presented in Table 3.

The Spectral Bit Capacity (SBC) and Spatial Bit Density (SBD) are evaluated through equations (14) and (15) respectively. These metrics are employed to analyze the frequency allocation and spatial requirements, respectively.

$$\text{SBC(bit/GHz)} = \frac{\text{number of bits}}{\text{frequency bandwith (GHz)}} \tag{14}$$

$$\text{SBD(bit/cm}^2\text{)} = \frac{\text{number of bits}}{\text{Tag size(cm}^2\text{)}} \tag{15}$$

Table 3 highlights the paramount significance of high spectral capacity when compared to other benchmarks. With a robust high spectral capacity of 9.6 bits/GHz, the system boasts the ability to accommodate an extensive range of unique identifiers, totaling 24 bits. This capability directly translates to the system's proficiency in seamlessly transmitting and receiving substantial volumes of data within the specified frequency range of 4-6.5 GHz. In the context of IoT applications, where numerous devices need to communicate wirelessly, having a higher spectral capacity allows for higher data throughput, reduced interference, improved scalability, and the ability to handle a larger number of unique identifiers. This is crucial as IoT systems generate vast amounts of data, and efficient communication is essential for their functionality.

VII. CONCLUSION

The development of chipless RFID tags tailored for IoT applications entails a comprehensive analysis encompassing aspects such as wireless connectivity, physical dimensions, data encoding, interference mitigation, coding capability, utilization of frequency spectrum, and overall operational efficiency. By addressing these factors, the designed chipless tag meet the specific demands of IoT systems, enabling efficient tracking and identification of items in a variety of industrial applications. The focus of this research centers on compact Radar Cross-Section (RCS)-based RFID chipless tags. Notably, these tags are characterized by their utilization of a slow-wave structure in their design. Despite their size of only 60 $\times$ 40 mm^2, these tags possess the remarkable capacity to encode 24 bits of information. A critical aspect of the research was the thoughtful arrangement of resonators, strategically designed to minimize frequency fluctuations arising from mutual coupling among the reflecting resonators. The experimental analysis, conducted with all bits set to 1, revealed the presence of 24 resonant frequencies distinguished by their high Q-factors and straightforward detectability.

REFERENCES

[1] A. Ayub Khan, A. A. Laghari, Z. A. Shaikh, Z. Dacko-Pikiewicz, and S. Kot, "Internet of Things (IoT) security with blockchain technology: A state-of-the-art review," *IEEE Access*, vol. 10, pp. 122679–122695, 2022.

[2] S. Faryad, H. Batool, M. Asif, and A. Yasin, "Impact of Internet of Things (IoT) as persuasive technology," *Int. J. Inf. Technol. Comput. Sci.*, vol. 13, no. 6, pp. 16–28, Dec. 2021.

[3] S. Kumar, P. Tiwari, and M. Zymbler, "Internet of Things is a revolutionary approach for future technology enhancement: A review," *J. Big Data*, vol. 6, no. 1, pp. 1–21, Dec. 2019.

[4] S. Mukhopadhyay, N. Suryadevara, and A. Nag, "Wearable sensors and systems in the IoT," *Sensors*, vol. 21, no. 23, p. 7880, Nov. 2021.

[5] Y. Perwej, M. K. Omer, O. E. Sheta, H. A. Harb, and M. S. Adrees, "The future of Internet of Things (IoT) and its empowering technology," *Int. J. Eng. Sci.*, vol. 9, no. 3, pp. 20192–20202, Mar. 2019.

[6] V. Sharma and M. Hashmi, "On the seamless integration and co-existence of chipless RFID in broad IoT framework," *IEEE Access*, vol. 9, pp. 69839–69849, 2021.

[7] A. Zahid, N. Mufti, S. Ullah, M. W. Nawaz, A. Sharif, M. A. Imran, and Q. H. Abbasi, "IoT-enabled vacant parking slot detection system using inkjet-printed RFID tags," *IEEE Sensors J.*, vol. 23, no. 7, pp. 7828–7835, Apr. 2023.

[8] L. Zhang, S. Rodriguez, H. Tenhunen, and L.-R. Zheng, "An innovative fully printable RFID technology based on high speed time-domain reflections," in *Proc. Conf. High Density Microsyst. Design Packag. Compon. Failure Anal. (HDP)*, 2006, pp. 166–170.

[9] M. El-Absi, A. Al-Haj Abbas, and T. Kaiser, "Chipless RFID tags placement optimization as infrastructure for maximal localization coverage," *IEEE J. Radio Freq. Identificat.*, vol. 6, pp. 368–380, 2022.

[10] R. S. Nair, E. Perret, S. Tedjini, and T. Baron, "A group-delay-based chipless RFID humidity tag sensor using silicon nanowires," *IEEE Antennas Wireless Propag. Lett.*, vol. 12, pp. 729–732, 2013.

[11] Z. Yang, K. Y. See, M. F. Karim, and A. Weerasinghe, "Chipless RFID-based sensing system for partial discharge detection and identification," *IEEE Sensors J.*, vol. 21, no. 2, pp. 2277–2285, Jan. 2021.

[12] C. S. Hartmann, "A global SAW ID tag with large data capacity," in *Proc. IEEE Ultrason. Symp., Proceedings.*, vol. 1, Oct. 2002, pp. 65–69.

[13] T. F. Bechteler and H. Yenigun, "2-D localization and identification based on SAW ID-tags at 2.5 GHz," *IEEE Trans. Microw. Theory Techn.*, vol. 51, no. 5, pp. 1584–1590, May 2003.

[14] V. P. Plessky and L. M. Reindl, "Review on SAW RFID tags," *IEEE Trans. Ultrason., Ferroelectr., Freq. Control*, vol. 57, no. 3, pp. 654–668, Mar. 2010.

[15] S. Preradovic, I. Balbin, N. C. Karmakar, and G. Swiegers, "A novel chipless RFID system based on planar multiresonators for barcode replacement," in *Proc. IEEE Int. Conf. RFID*, Apr. 2008, pp. 289–296.

[16] S. Preradovic and N. C. Karmakar, "Design of fully printable planar chipless RFID transponder with 35-bit data capacity," in *Proc. Eur. Microw. Conf. (EuMC)*, Sep. 2009, pp. 13–16.

[17] I. Jalaly and I. D. Robertson, "RF barcodes using multiple frequency bands," in *IEEE MTT-S Int. Microw. Symp. Dig.*, Jun. 2005, pp. 139–142.

[18] A. Vena, E. Perret, and S. Tedjini, "A fully printable chipless RFID tag with detuning correction technique," *IEEE Microw. Wireless Compon. Lett.*, vol. 22, no. 4, pp. 209–211, Apr. 2012.

[19] A. Vena, E. Perret, and S. Tedjini, "High-capacity chipless RFID tag insensitive to the polarization," *IEEE Trans. Antennas Propag.*, vol. 60, no. 10, pp. 4509–4515, Oct. 2012.

[20] A. Vena, E. Perret, and S. Tedjini, "Chipless RFID tag using hybrid coding technique," *IEEE Trans. Microw. Theory Techn.*, vol. 59, no. 12, pp. 3356–3364, Dec. 2011.

[21] F. Babaeian and N. C. Karmakar, "Hybrid chipless RFID tags—A pathway to EPC global standard," *IEEE Access*, vol. 6, pp. 67415–67426, 2018.

[22] M. Hayati, S. Majidifar, and S. N. Sobhani, "Using a hybrid encoding method based on the hexagonal resonators to increase the coding capacity of chipless RFID tags," *Int. J. RF Microw. Comput.-Aided Eng.*, vol. 32, no. 12, Dec. 2022.

[23] A. Jiménez-Sáez, M. Schüßler, M. Nickel, and R. Jakoby, "Hybrid time-frequency modulation scheme for chipless wireless identification and sensing," *IEEE Sensors J.*, vol. 18, no. 19, pp. 7850–7859, Oct. 2018.
[24] A. Vena, A. A. Babar, L. Sydänheimo, M. M. Tentzeris, and L. Ukkonen, "A novel near-transparent ASK-reconfigurable inkjet-printed chipless RFID tag," *IEEE Antennas Wireless Propag. Lett.*, vol. 12, pp. 753–756, 2013.
[25] K. Mekki, O. Necibi, and A. Gharsallah, "Design of a miniaturized dipole RFID tag antenna," *Indian J. Sci. Technol.*, vol. 13, no. 30, pp. 3103–3112, 2020.
[26] K. Mekki, O. Necibi, C. Boussetta, and A. Gharsallah, "Miniaturization of circularly polarized patch antenna for RFID reader applications," *Eng., Technol. Appl. Sci. Res.*, vol. 10, no. 3, pp. 5655–5659, Jun. 2020.
[27] K. Mekki, C. Boussetta, and A. Gharsallah, "Design and miniaturization of UHF RFID reader antenna," in *Proc. 18th Medit. Microw. Symp. (MMS)*, Oct. 2018, pp. 9–12.
[28] K. Mekki, O. Necibi, S. Lakhdhar, and A. Gharsallah, "A UHF/UWB monopole antenna design process integrated in an RFID reader board," *J. Electromagn. Eng. Sci.*, vol. 22, no 4, pp. 479–487, 2022.
[29] K. Mekki, O. Necibi, H. Dinis, P. Mendes, and A. Gharsallah, "Backscatter analysis in UWB chipless RFID based on UWB-IR," in *Proc. IEEE Texas Symp. Wireless Microw. Circuits Syst. (WMCS)*, May 2021, pp. 1–5.
[30] K. Mekki, O. Necibi, W. El May, K. Rabaani, and A. Gharsallah, "Design of a UHF/UWB monopole antenna integrated in an RFID reader board," in *Proc. IEEE 19th Int. Symp. Antenna Technol. Appl. Electromagn. (ANTEM)*, Aug. 2021, pp. 1–2.
[31] K. Mekki, O. Necibi, H. Dinis, P. Mendes, and A. Gharsallah, "Chipless RF identification tags with microstrip patch resonators," *Microw. J.*, vol. 65, no. 11, pp. 58–72, 2022.
[32] K. Mekki, O. Necibi, H. Dinis, P. Mendes, and A. Gharsallah, "Investigation on the chipless RFID tag with a UWB pulse using a UWB IR-based reader," *Int. J. Microw. Wireless Technol.*, vol. 14, no. 2, pp. 166–175, Mar. 2022.
[33] M. E. Jalil, M. K. A. Rahim, N. A. Samsuri, and R. Dewan, "Chipless RFID tag based on meandered line resonator," in *Proc. IEEE Asia–Pacific Conf. Appl. Electromagn. (APACE)*, Dec. 2014, pp. 203–206.
[34] K. W. Eccleston and S. H. M. Ong, "Compact planar microstripline branch-line and rat-race couplers," *IEEE Trans. Microw. Theory Techn.*, vol. 51, no. 10, pp. 2119–2125, Oct. 2003, doi: 10.1109/TMTT.2003.817442.
[35] J. S. Hong and M. J. Lancaster, "Capacitively loaded microstrip loop resonator," *Electron. Lett.*, vol. 30, no. 18, pp. 1494–1495, Sep. 1994, doi: 10.1049/el:19941025.
[36] K. Rawat and F. M. Ghannouchi, "A design methodology for miniaturized power dividers using periodically loaded slow wave structure with dual-band applications," *IEEE Trans. Microw. Theory Techn.*, vol. 57, no. 12, pp. 3380–3388, Dec. 2009, doi: 10.1109/TMTT.2009.2033849.
[37] C. Zhou and H. Y. D. Yang, "Design considerations of miniaturized least dispersive periodic slow-wave structures," *IEEE Trans. Microw. Theory Techn.*, vol. 56, no. 2, pp. 467–474, 2008, doi: 10.1109/TMTT.2007.914633.
[38] J. Machac, A. Boussada, M. Svanda, J. Havlicek, and M. Polivka, "Influence of mutual coupling on stability of RCS response in chipless RFID," *Technologies*, vol. 6, no. 3, p. 67, Jul. 2018.
[39] M. Polivka, J. Havlicek, M. Svanda, and J. Machac, "Improvement in robustness and recognizability of RCS response of U-shaped strip-based chipless RFID tags," *IEEE Antennas Wireless Propag. Lett.*, vol. 15, pp. 2000–2003, 2016.
[40] H. Ayadi, J. Machac, M. Svanda, N. Boulejfen, and L. Latrach, "Proof of concept of reconfigurable solvent vapor sensor tag with wireless power transfer for IoT applications," *Appl. Sci.*, vol. 12, no. 20, p. 10266, Mar. 2022.
[41] R. Rezaiesarlak and M. Manteghi, "Design of chipless RFID tags based on characteristic mode theory (CMT)," *IEEE Trans. Antennas Propag.*, vol. 63, no. 2, pp. 711–718, Feb. 2015.
[42] Md. A. Islam and N. C. Karmakar, "A novel compact printable dual-polarized chipless RFID system," *IEEE Trans. Microw. Theory Techn.*, vol. 60, no. 7, pp. 2142–2151, Jul. 2012.
[43] D. Betancourt, K. Haase, A. Hübler, and F. Ellinger, "Bending and folding effect study of flexible fully printed and late-stage codified octagonal chipless RFID tags," *IEEE Trans. Antennas Propag.*, vol. 64, no. 7, pp. 2815–2823, Jul. 2016.
[44] M. Svanda, J. Havlicek, J. Machac, and M. Polivka, "Polarisation independent chipless RFID tag based on circular arrangement of dual-spiral capacitively-loaded dipoles with robust RCS response," *IET Microw., Antennas Propag.*, vol. 12, no. 14, pp. 2167–2171, Nov. 2018.
[45] Md. A. Islam and N. C. Karmakar, "Compact printable chipless RFID systems," *IEEE Trans. Microw. Theory Techn.*, vol. 63, no. 11, pp. 3785–3793, Nov. 2015.
[46] A. Vena, E. Perret, and S. Tedjini, "Depolarizing chipless RFID tag for robust detection and its FCC compliant UWB reading system," *IEEE Trans. Microw. Theory Techn.*, vol. 61, no. 8, pp. 2913–2924, Jun. 2013.
[47] O. Rance, R. Siragusa, P. Lemaître-Auger, and E. Perret, "Toward RCS magnitude level coding for chipless RFID," *IEEE Trans. Microw. Theory Techn.*, vol. 64, no. 7, pp. 2315–2325, Jul. 2016.
[48] M. Khaliel, A. El-Awamry, A. Fawky Megahed, and T. Kaiser, "A novel design approach for Co/cross-polarizing chipless RFID tags of high coding capacity," *IEEE J. Radio Freq. Identificat.*, vol. 1, no. 2, pp. 135–143, Jun. 2017.
[49] K. Mekki, O. Necibi, H. Dinis, P. Mendes, and A. Gharsallah, "Frequency-spectra-based high coding capacity chipless RFID using an UWB-IR approach," *Sensors*, vol. 21, no. 7, p. 2525, Apr. 2021.
[50] V. Sharma, S. Malhotra, and M. Hashmi, "Slot resonator based novel orientation independent chipless RFID tag configurations," *IEEE Sensors J.*, vol. 19, no. 13, pp. 5153–5160, Jul. 2019.
[51] M. Added, N. Boulejfen, M. Svanda, F. M. Ghannouchi, and T.-P. Vuong, "High-performance chipless radio-frequency identification tags: Using a slow-wave approach for miniaturized structure," *IEEE Antennas Propag. Mag.*, vol. 61, no. 4, pp. 46–54, Aug. 2019.
[52] Y. Ni, X. Huang, Y. Lv, and C. Cheng, "Hybrid coding chipless tag based on impedance loading," *IET Microw., Antennas Propag.*, vol. 11, no. 10, pp. 1325–1331, Aug. 2017.
[53] J. Kracek, M. Svanda, and K. Hoffmann, "Scalar method for reading of chipless RFID tags based on limited ground plane backed dipole resonator array," *IEEE Trans. Microw. Theory Techn.*, vol. 67, no. 11, pp. 4547–4558, Nov. 2019.
[54] N. Tariq, M. A. Riaz, H. Shahid, M. J. Khan, M. S. Khan, Y. Amin, J. Loo, and H. Tenhunen, "Orientation independent chipless RFID tag using novel trefoil resonators," *IEEE Access*, vol. 7, pp. 122398–122407, 2019.
[55] F. Costa, S. Genovesi, and A. Monorchio, "A chipless RFID based on multiresonant high-impedance surfaces," *IEEE Trans. Microw. Theory Techn.*, vol. 61, no. 1, pp. 146–153, Jan. 2013.

KAWTHER MEKKI (Graduate Student Member, IEEE) received the integrated master's degree in electronics, electrotechnics, and automation from the Faculty of Science of Tunis, University of Tunis El Manar, Tunisia, in 2016. She is currently pursuing the Ph.D. degree with the Laboratory for Research on Microwave Electronics, University of Tunis El-Manar. Her research interests include the design and development of antennas for chipless RFID tags.

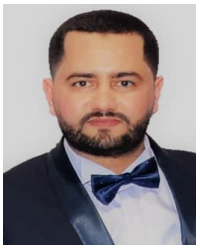

OMRANE NECIBI received the M.Sc. degree in analysis and digital processing of electronic systems and the Ph.D. degree in sciences and technology from the Faculty of Science of Tunis, University of Tunis El-Manar, Tunisia, in 2012 and 2015, respectively. He is currently an Assistant Professor with the Department of Computer Science, College of Arts and Sciences at Tabarjal, Jouf University, Saudi Arabia. His research interest includes wireless communication, in particular radio-frequency identification (RFID) with the design and development of antennas for chipless RFID tags.

NOUREDDINE BOULEJFEN (Senior Member, IEEE) received the B.S. degree in electrical engineering from École nationale d'ingénieurs de Monastir, Monastir, Tunisia, in 1993, and the M.S. and Ph.D. degrees in microwave engineering from École Polytechnique de Montréal, Montreal, QC, Canada, in 1996 and 2000, respectively. In 2000, he joined the Micro-Electronics Group, Department of Fiber Optic, Nortel Networks Inc., Ottawa, ON, Canada, where he was an Engineer with the On-Wafer Test and Characterization Laboratory, until 2002. From 2003 to 2011, he was an Assistant Professor with the Department of Electrical Engineering, University of Hail, Hail, Saudi Arabia, and the University of Kairouan, Kairouan, Tunisia, until 2016. He is currently a Full Professor with the Centre for Research on Microelectronics and Nanotechnology, Sousse, Tunisia. His research interests include the design, modeling, optimization, and linearization of RF power amplifiers, the design of microwave passive components using SIW technology, and the design and calibration of microwave passive receivers.

SAMIA LARGUECH received the Ph.D. degree in electrical engineering-automatic from the University of Picardie Jules Verne and the National School of Engineering of Sfax, in 2017. Since 2018, she has been an Assistant Professor and the Head of the Department of Electrical Engineering, College of Engineering, Princess Nourah bint Abdulrahman University, Riyadh, Saudi Arabia. Her research interests include fuzzy control, vehicle dynamics, fault-tolerant control, neural networks, adaptive control, sliding mode control, and diesel engines.

NORAH MUHAMMAD ALWADAI received the M.Sc. degree in solid state physics from King Saud University, Riyadh, Saudi Arabia, in 2012, and the Ph.D. degree in material science and engineering from the Semiconductor and Material Spectroscopy Group, King Abdullah University of Science and Technology (KAUST), Thuwal, in 2019. She is currently an Assistant Professor with the Department of Physics, Princess Nourah bint Abdulrahman University, Riyadh. Her research interests include semiconductor nanostructure (mainly ZnO and GaN-related materials) functionalized by emerging materials for optoelectronic devices. She received the Princess Nourah bint Abdulrahman Award for research excellence for the university's scholarships and postgraduate studies, in 2020.

ALI GHARSALLAH (Senior Member, IEEE) received the degree in radio-frequency engineering from the Higher School of Telecommunication of Tunis, in 1986, and the Ph.D. degree from the Engineering School of Tunis, in 1994. Since 1991, he has been with the Department of Physics, Faculty of Sciences of Tunis, University of Tunis El Manar. He is also a Full Professor of electrical engineering and the Director of Engineering with the Ministry of Higher Education of Tunisia. He has authored or coauthored approximately 100 papers published in scientific journals and 120 conference papers. He has also supervised more than 20 theses and 50 master's research projects. His current research interests include smart antennas, array signal processing, multilayered structures, and microwave-integrated circuits.